Journal of Structural Geology, Vol. 10, No. 2, pp. 193 to 199, 1988
Printed in Great Britain

0191-8141/88 $03.00 + 0.00

Paleostress determination in a rock by a fractographic method

DOV BAHAT* and A. RABINOVITCH†

*Department of Geology and Mineralogy and †Department of Physics, The Ben Gurion University of the Negev, Beer Sheva, Israel

(*Received* 30 *April* 1987; *accepted in revised form* 30 *November* 1987)

Abstract—A fractographic technique, hitherto used in ceramics for the evaluation of fracture stress, is adapted here to calculate fracture paleostresses in rocks. An example from a granite in East Sinai is analyzed. The results obtained for the ranges of local paleofracture stress, the severest flaw size and the initial stress intensity factor agree reasonably well with previous evaluations of fracture stresses in granite and with direct observations of the rock's grain size.

INTRODUCTION

FRACTOGRAPHY is the study of fracture processes by means of surface morphology. By the late 19th century geologists recognized that the feather patterns on joint surfaces contained information about the process of fracture propagation in rocks (Woodworth 1896). Various fracture surface features were distinguished. These were axial, radial and circular 'plumes' and 'rib-marks' with similarities to fracture morphologies in glasses and ceramics (e.g. Hodgson 1961, Bankwitz 1966, Kulander *et al.* 1979). Quantitative parameters of fracture mechanics were successfully derived from fracture morphologies in ceramics (Bansal & Duckworth 1977). Although the application of similar techniques to geological problems appeared to be a promising endeavor (Bahat 1979, Norton & Atkinson 1981) the feasibility of such a calculation has not been demonstrated so far.

Studies of fracture markings on joint surfaces have been confined mostly to sedimentary rocks (e.g. Kulander *et al.* 1979) and were limited to qualitative characterizations. The present study offers an explicit method based on fractographic parameters for the determination of the local paleostress which caused a fracture in a rock. As an exercise we analyze a specific fracture in an unroofed granite from East Sinai in order to show that this method can in fact be utilized for such an analysis. It should be emphasized however, that the numerical results obtained are only indicative and call for additional supportive data for a final evaluation of the examined paleostress.

FRACTURE MODEL

Fractures in rocks extend from pre-existing flaws. Those which are responsible for failure are the severest material flaws of initial length $2c_i$ (Fig. 1) and are usually taken to be the longest (and straightest) of its grain boundaries (Friedman & Logan 1970). Another important parameter is the critical crack half length c_{cr} (Fig. 1). The diameter $2c_{cr}$ marks the perimeter at which subcritical crack growth transforms to rapid fracture propagation and mixed mode stresses are replaced by a single mode I fracture (Fig. 2). There are three distinct zones on a fractured surface beyond c_{cr}: a smooth one called the *mirror plane*, perpendicular to the applied tensile stress, which extends from c_{cr} to r_m; an arc of stippled surface known as the *mist*, extending to r; and a rougher region, termed *hackle*, with radiating cracks farther from the origin up to r_b (Holloway 1973, Mecholsky & Freiman 1979). Many investigators (e.g. Bansal 1977) have obtained the semi-empirical formula

$$\sigma_f = A_j r_j^{-1/2}, \tag{1}$$

where σ_f is the fracture stress, r_j is the distance to a particular boundary and A_j is the corresponding mirror constant. It should be emphasized that if A_j can be defined, the paleostress σ_f can be determined by measuring r_j.

Following Mecholsky & Freiman (1979) we define K_{Ic} as the stress intensity factor at which the crack starts to grow catastrophically. An exact form for K_{Ic} in our case is given by:

$$K_{Ic} = (1.2\pi/Q)^{1/2}\sigma_f c_{cr}^{1/2}, \tag{2}$$

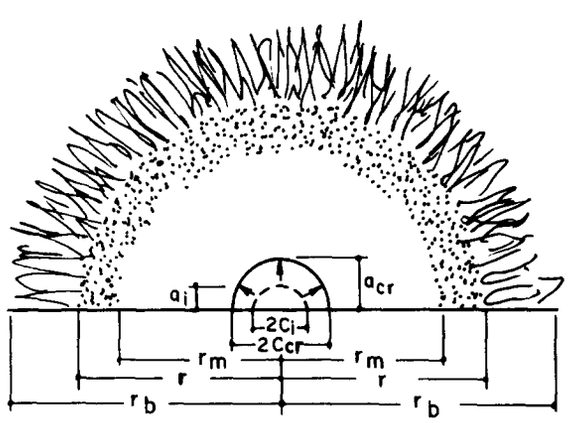

Fig. 1. Schematic fracture surface of brittle materials showing idealized initial flaw length $2c_i$ and depth a_i, critical flaw length $2c_{cr}$ and depth a_{cr}. The three mirror radii r_m (mirror–mist boundary), r (mist–hackle boundary and r_b (initiation of macroscopic crack branching) are shown also (after Mecholsky & Freiman 1979).

where Q is a modifying geometrical factor ranging in value from 1.0 for a long shallow flaw to 2.46 for a semi-circular flaw (Randall 1966) and 1.2 is the coefficient of surface flaw. Since we do not know the shape of the flaw, the calculation is carried out for these two extreme Q values.

The present analysis is based on the following assumptions (see Discussion):

(1) fracture mechanics analyses of glass and ceramics may be adapted to the fracture of brittle solid rocks. Although the processes taking place in rock fracture are more complex because of pore pressure, inhomogeneities and non-linearities (Peck *et al.* 1985), effective elastic parameters can be defined. Such parameters are used in the following analysis, but complexities may lead to a higher error in the final result;

(2) initial fracture propagation occurs under sub-critical stress intensity conditions ($K_I < K_{Ic}$);

(3) as the fracture length c reaches the critical size c_{cr} (K_I attains the value K_{Ic}) spontaneous propagation starts;

(4) post-critical fracture takes place under constant tensile stress with a negligible pore pressure effect.

DETERMINATION OF FRACTURE STRESS

We determine the fracture stress by two methods. The first is based on the ratio of the mist–hackle radius r to c_{cr} (Fig. 1). This ratio has been theoretically implied (Anthony & Congleton 1968) and empirically shown (Bansal 1977, Mecholsky & Freiman 1979) to be a constant for various glass and ceramic materials. This method is not directly related to the fracture geometry since c_{cr} must be determined empirically from the radius r (see equation 3 below) which may cause an increased error. The second method, on the other hand, directly uses the radius r together with Griffith's equation modified for bifurcations by Congleton & Petch (1967). The straightforward manner in which geometry and stress are related considerably reduces errors; hence this is usually the preferred method. This point is clearly demonstrated in the example treated below. While the first method only yields an order of magnitude estimation of the paleostress, the second method determines it to within a reasonable range.

First method

In ceramic and rock materials the mist band is generally not observed (due to the material graininess). The constant r/c_{cr} in ceramics is 16.7 according to Mecholsky & Freiman (1979, table 3, no error bars are provided). A different value for this ratio, which applies to glass ceramics, is 13.9 (Bansal 1977, equation 3 and table 2):

$$A_m/K_{Ic} = B(r_m/c_{cr})^{1/2} = 2.39, \quad (3)$$

where B is a geometrical constant (=0.74 for semi-circular surface flaws which are much smaller than the specimen thickness) and A_m is the mirror–mist constant. As the first method uses r/c_{cr}, we have to multiply the r_m/c_{cr} value (which by equation 3 is 10.4) by r/r_m. The average ratio r/r_m is 1.34 according to Mecholsky & Freiman (1979, table 3), hence $r/c_{cr} = 13.9$. In the analysis that follows, we will use both of these values for r/c_{cr} in obtaining approximate bounds for σ_f.

Second method

Hackling is the consequence of fracture branching. According to Congleton & Petch (1967, their equation 3 modified) this branching occurs when

$$\sigma_f = 2G(E\gamma/\pi)^{1/2}r^{-1/2} \quad (4)$$

where E, γ and G are Young's modulus, the surface energy and the enhancement factor for fast vs slow propagation (see below), respectively. Using relevant estimates for these constants, equation (4) yields σ_f directly.

Sub-critical and post-critical fracture propagation

The propagation history of the crack in the Sinai granite (Fig. 3) consists of two stages, the sub-critical crack growth and the post-critical one. The observed hackling (bifurcation, Fig. 3) indicates that the fracture advanced rapidly during the post-critical stage without any periods of rhythmic increase and decrease of stresses (Secor 1969). It is therefore reasonable to assume that this propagation occurred under pure tensile effective stress with negligible pore pressure influence. Experimental evidence for the lack of influence of water upon crack propagation at high velocities (region III) was obtained by Wiederhorn (1967), where at such velocities the same behaviour was observed for different water concentrations. It is clear that water cannot percolate into the crack tip at these high crack velocities (Secor 1969). The tensile stress could have been the consequence of the uplifting in the area (Kohn & Eyal 1981) and would have been caused by the mechanism envisaged by Voight & St. Pierre (1974).

On the other hand, during the sub-critical stage a periodic increase and decrease of pore pressure could have occurred at depth, under considerable overburden pressures.

Initial microcrack propagation

During the sub-critical stage the effective minimum stress $\bar{\sigma}$ is the sum of the total minimum stress and the pore pressure. If both the duration of this stage and $\bar{\sigma}$ can be estimated even approximately, c_i and K_{Ii} (the initial stress intensity factor) can be calculated.

According to Charles (1958), in the sub-critical crack growth regime:

$$V = WK_I^n, \quad (5)$$

where V is the crack velocity, K_I is the instantaneous stress intensity factor $K_I = \bar{\sigma}(1.2\pi c/Q)^{1/2}$, with c the instantaneous crack radius. W and n are temperature-

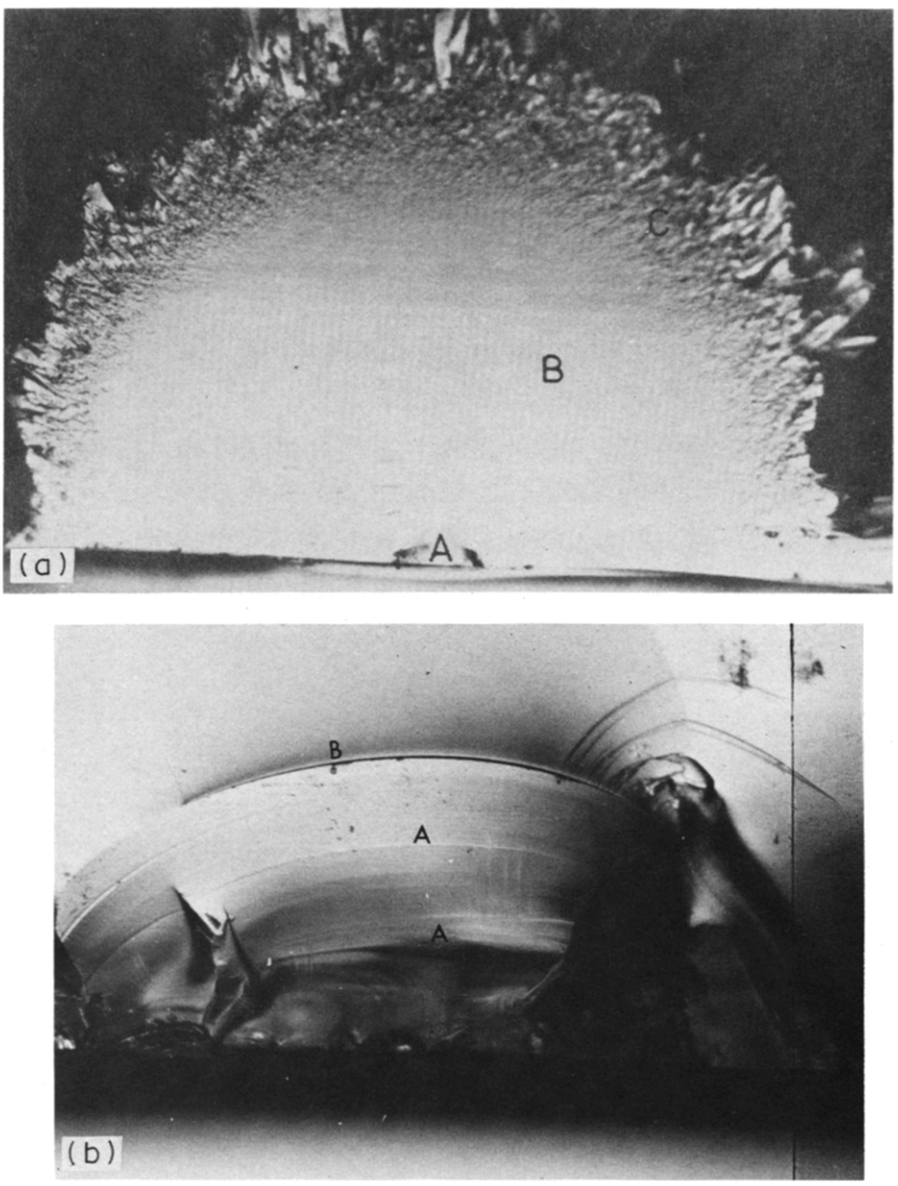

Fig. 2. Experimental results of fractured glass. (a) A mirror plane B with the critical flaw A at the lower center, surrounded by arcs of mist and hackle C; length of mirror diameter is 9 mm. (b) Initial flaw with early concentric undulations A at sub-critical stage and critical perimeter B at transition to catastrophic fracture (after Bahat *et al.* 1982).

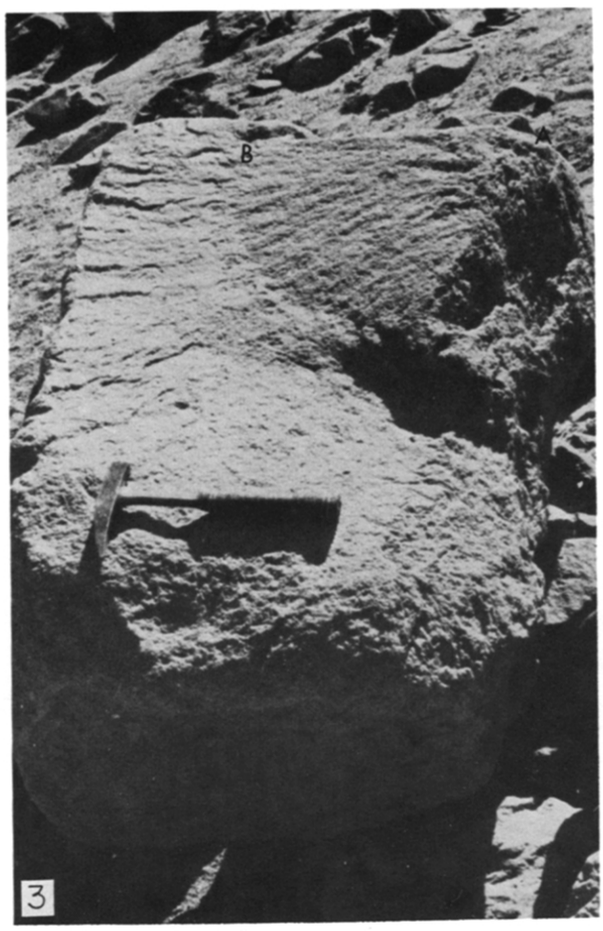

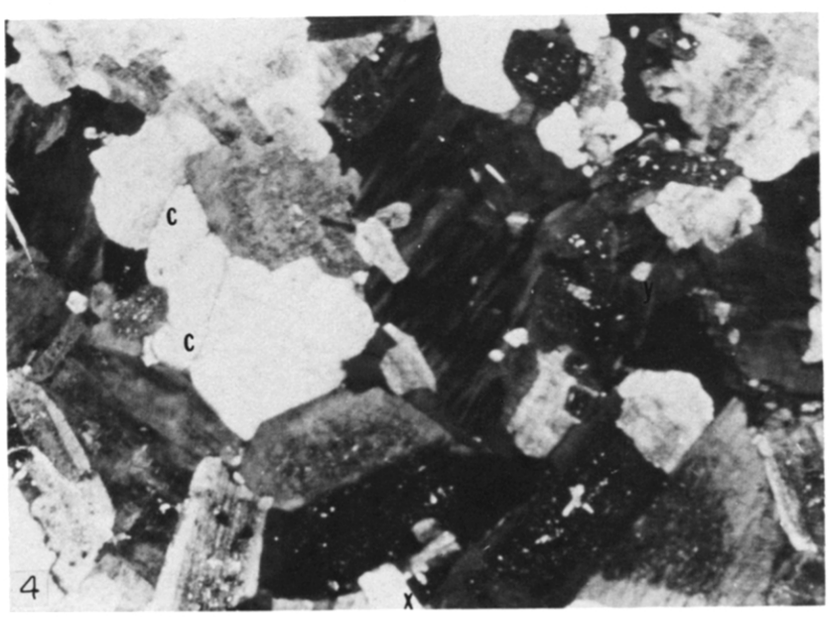

Fig. 3. Fracture surface in granite from Eastern Sinai; fracture initiation at A. Curve B marks the circular perimeter of the hackle boundary (the mirror–mist boundary from Figs. 1 and 2 is not visible due to rock graininess). Note radial striations between A and B and hackles beyond B. Distance between A to B, $r = 360$ mm.

Fig. 4. Thin section of granite from Eastern Sinai. A micro-crack 4 mm long (see distance between x and y) along the boundary between two feldspars (dark) is depicted. Two micro-cracks across a quartz grain (white) are seen as well (near letter c). Crossed nicols.

dependent constants. Integrating equation (5) with respect to time for constant $\bar{\sigma}$ yields (Wiederhorn *et al.* 1974):

$$c_i^{[(n/2)-1]} = 2/[W\bar{\sigma}^n(n-2)\Delta t(1.2\pi/Q)^{n/2}], \quad (6)$$

where Δt is the time elapsed between the initiation of sub-critical crack growth and the transition to catastrophic propagation. For self-consistency of this calculation, the obtained c_i value should be of the order of the grain size of the analyzed material. The initial stress intensity factor K_{Ii} can be calculated by

$$K_{Ii} = (1.2\pi/Q)^{1/2}\bar{\sigma}c_i^{1/2}. \quad (7)$$

AN EXAMPLE: EAST SINAI GRANITE

Fracture markings and micro-cracks

Fracture markings commonly occur on surfaces of fine-grained rocks like chalks, sandstones, slates and even lavas or hypabyssal rocks. They are rare in medium-grained rocks like granite owing to the increased effect of grain boundaries in masking the delicate fracture morphology. Exceptionally well developed fracture markings on a joint in granite (Fig. 3) were found in Wadi Zrara in Eastern Sinai at co-ordinates 28°40′/34°17.5′.

The granite jointing is ascribed to the great uplift that started in the late Neogene (Garfunkel & Bartov 1977, Bahat 1980) with an approximate rate of 0.1–0.2 mm yr^{-1} (Kohn & Eyal 1981).

The extreme upper right side of the granitic block is the point of fracture initiation (Fig. 3, point A). The radial striations suggest that the fracture propagated radially from right to left, producing a concentric curve (curve B) which marks the circular boundary of the mirror plane. To the left of this boundary a region of hackles is developed. A distinction can be made between the radial striations on the mirror plane, which although clearly visible are rather superficial, and the quasi-radial marks in the hackle region which show considerably deeper cracks in the rock.

The granite investigated has an equigranular fine to medium-grained texture (Fig. 4). Microscopic examination reveals micro-cracks along the grain boundaries, typically between quartz and feldspar grains (Fig. 4). Occasionally micro-cracks cross quartz crystals and may occur as two or three dimensional anastomosing networks. Fractures can also be traced along several adjacent biotite grains. Straight or arced traces that follow such micro-crack patterns (ignoring short curvatures) reach approximate lengths of 4 mm. Accordingly, the measured $2c_i$ ranges from 4 to 5 mm (the latter is the maximum straight grain boundary of quartz).

Fracture growth and loading rate

Crack propagation seeks paths of minimum fracture toughness. Fracture toughness is proportional to the surface energy which is considerably lower for mica (0.45 Jm^{-2}, Bryant *et al.* 1963) than for microcline (4.06 Jm^{-2}, Atkinson & Avdis 1980) and quartz (0.41–1.34 Jm^{-2}, Brace & Walsh 1962, Atkinson & Avdis 1980).

Presumably, therefore, sub-critical fracture propagation in granite occurs initially along mica flakes, quartz crystals or grain boundaries. At some stage the stress intensity K_I at the tip of the crack reaches the value of fracture toughness along these paths and possibly the propagation velocity increases. Eventually, the crack tip reaches a feldspar grain, and as the fracture toughness of feldspar is higher, two alternative developments are possible. Fracture length (equation 2) may be high enough (through quartz, along mica flakes or grain boundaries) to enable critical fracture to continue into the feldspar (when K_{Ic} of feldspar is reached). However, if the fracture length is too short or there are too few interconnected mica or quartz grains for such a development to occur, the crack would stop at a feldspar boundary.

A transition to critical propagation in felspar, being dependent on conditions of stress corrosion, may or may not be reached. Stress corrosion may enable sub-critical propagation through feldspar or along feldspar boundaries following the above mentioned arrest. If the fracture toughness of feldspar is eventually reached, a critical fracture propagation would then occur in feldspar and continue through the entire rock producing a joint. Furthermore, if K_I gets to be high enough to initiate bifurcation (a little above $2K_{Ic}$, Anthony & Congleton 1968, Bansal 1977) hackles would develop (see Discussion).

The morphology of the cracked surface is dependent on the loading rate. We consider three different loading rates and their derived morphologies.

(1) For a high loading rate $c_{cr} \cong c_i$, and thus, the observed flaw perimeter represents both c_i and c_{cr}.

(2) For medium loading rates (Bahat *et al.* 1982), several transitional stages can be observed from c_i to a larger c_{cr} (Fig. 2). Both c_i and c_{cr} are discernible.

(3) Under slow rates (sub-critical conditions) these transitions are gradual and could even be unobservable. In the latter situation it would be impossible to directly evaluate c_{cr}; only c_i could be discerned.

Sub-critical growth of the flaw can take place under different conditions of stress corrosion and loading rates such that c_{cr}/c_i ratio can be $\gg 1$. Size differences between c_{cr} and c_i have repeatedly been observed (Bansal & Duckworth 1977, Mecholsky & Freiman 1979, Bahat *et al.* 1982).

σ_f determination by first method

The mist–hackle radius r in the granite is 360 mm (Fig. 3). This radius is the distance between the flaw origin and the initiation of hackle (Fig. 1). The critical flaw radius c_{cr} is determined to be 22 mm for $r/c_{cr} = 16.7$ and 26 mm for $r/c_{cr} = 13.9$. The fracture toughness of granite is highly variable and K_{Ic} values range between 0.9 and 2.9

Table 1. Determination of fracture stress in jointing of granite from Sinai

K_{Ic} (MPam$^{1/2}$)	σ_f c_{cr} = 26 mm		σ_f c_{cr} = 22 mm	
	Shallow flaw	Semi-circular flaw	Shallow flaw	Semi-circular flaw
0.9	2.9	4.6	3.1	4.9
2.9	9.2	14.4	10.1	15.8
1.9	6.0	9.4	6.7	10.5

Fracture stress results for three values of K_{Ic} are given in MPa.

MPam$^{1/2}$ (Atkinson 1984, fig. 18). We therefore calculate σ_f for these two values as well as for their average = 1.9 MPam$^{1/2}$. Using equation (2), σ_f ranges between 2.9 and 10.1 MPa (Table 1) with an average of 6.5 MPa for a shallow flaw and between 4.6 and 15.8 MPa with an average of 10.2 MPa for a semi-circular flaw.

σ_f determination by second method

The values used are: $E = 5.0 \times 10^{10}$ Pa (Segall & Pollard 1983); $\gamma = 4.06$ Jm^{-2} for microcline (Atkinson & Avdis 1980). Here we have assumed that branching occurred in the feldspars (see Discussion). G ranges between $2\sqrt{2}$ and $5\sqrt{2}$ (Congleton & Petch 1967, p. 758). This yields the range $2.4 < \sigma_f < 6.0$ MPa, with an average of 4.2 MPa, which is reasonably close to the range obtained by the first method.

Initial stress intensity factor

Although it has been suggested that a lower limit for a crack growth must exist (Atkinson 1984), Wilkins (1980) found no such limit in the Lac du Bonnet granite, even for crack velocities as low as 10^{-12} ms^{-1}. Moreover, other studies of rocks have also failed to show crack growth limit at velocities of 10^{-9} ms^{-1} (Atkinson 1984). Therefore, we derive $\log_{10} W$ and n from Wilkins (1980). If, however, an experimental lower limit for granite is obtained, this part of our calculation would have to be modified. The values we use are therefore $n = 55/9$ and $\log_{10} W = -338$. We assume Δt to be of the order of 10 Ma since most of the domal uplift in Sinai post-dated 9 Ma, although it possibly started about 27 Ma ago (Kohn & Eyal 1981). Note that the results obtained from equation 6 are almost insensitive to Δt within these limits.

The values obtained for c_i as a function of $\bar{\sigma}$ (Table 2) show quite clearly that the estimate of 6.0 MPa for $\bar{\sigma}$ for a shallow flaw (or 9.4 MPa for a semi-circular one) has a reasonably good fit with the observed grain boundary size ($2c_i$ ranges from 4 to 5 mm). The magnitude of $\bar{\sigma}$ obtained seems therefore to be within the range of σ_f derived by the two methods. Owing to the crudity of the assumptions this agreement calls for additional confirmation.

Table 2. Initial micro-crack half lengths (c_i) for different assumed effective fracture stresses ($\bar{\sigma}$) for Sinai Eastern granite*

$\bar{\sigma}$ (MPa)	3.0	6.0	9.0
c_i (mm)	8.3	1.9	0.85

* The c_i values do not change for different flaw shapes since it depends upon $\bar{\sigma}/\sqrt{Q}$ (equation 6) which is shape-independent.

This calculated value of $c_i = 1.9$ mm requires in equation (7) an initial stress intensity factor of 0.51 MPam$^{1/2}$, which is about 4 times lower than the average K_{Ic} used.

DISCUSSION

In the Eastern Sinai granite, c_i was inferred to be approximately 2–2.5 mm, which should represent the longest 'Griffith crack' in the investigated material. Due to slow fracture propagation in the rock, however, K_{Ic} was reached only at $c_{cr} \simeq 24$ mm.

Our σ_f results which range between 3.0 and 16 MPa are generally lower than previous laboratory determinations of the tensile strength of granite (Segall & Pollard 1983, fig. 10). This could, however, be expected since the latter results were obtained under relatively fast loading rates, whereas fracture under the present investigation probably took place under prolonged fatigue conditions, which resulted in a lower fracture stress (Mould & Southwick 1959). Similar differences have already been observed (McGill & Stromquist 1979).

In spite of the relatively low stresses, once the critical fracture length c_{cr} was reached and crack propagation became rapid, the main features of fracture morphology were no longer affected by grain boundaries; thus the well-defined fractographic pattern shown in Fig. 3 is produced. It should perhaps be noted that fracture toughness of rock, that is, the transition to catastrophic crack propagation under quasi-static conditions, is not directly dependent on the measured c_i.

Regarding the calculation of σ_f by the second method, it was assumed that branching had occurred in feldspar. We now consider the alternatives. Had branching occurred in mica or quartz due to lower free surface energies in these materials, it is conceivable that the separate cracks would be unable to propagate through the feldspar when reaching the mica–feldspar interface, since K_I would be too low. The dynamic stress intensity factor drops considerably on branching (Kobayashi *et al.* 1974). Therefore, the new K_I of the individual branches, while being sufficient for crack propagation in mica (or quartz), would probably fail to cause propagation in feldspar. Instead, on reaching the boundary, the branches would advance along the mica–feldspar interface. Their eventual interaction might increase their mutual K_I, thus enabling the coalesced fracture to re-enter the feldspar (with a probable angular deflection). If we had allowed branching to initiate in either mica, quartz or feldspar, then perhaps more reasonable bounds of σ_f (from 0.8 to 8.3 MPa) would have been obtained.

In conclusion, it should be stressed that the granite

sample was only used to demonstrate the feasibility of the method for local stress determination even for relatively coarse grained material. An accurate evaluation of paleostresses in an investigated area should obviously require a series of fractographic analyses of many different joints.

REFERENCES

Anthony, S. R. & Congleton, J. 1968. Crack branching in strong metals. *Metal Sci. J.* **2**, 158–160.

Atkinson, B. K. 1984. Subcritical crack growth in geological minerals. *J. geophys. Res.* **89**, 4077–4114.

Atkinson, B. K. & Avdis, V. 1980. Fracture mechanics parameters of some rock forming minerals determined using an indentation technique. *Int. J. Rock Mech. & Mining Sci.* **17**, 383–386.

Bahat, D. 1979. Theoretical considerations on mechanical parameters of joint surfaces based on studies on ceramics. *Geol. Mag.* **116**, 81–92.

Bahat, D. 1980. A 'giant' plumose marking in Paleozoic sandstones from Sinai. *Tectonophysics* **68**, T1–T7.

Bahat, D., Leonard, G. & Rabinovitch, A. 1982. Analysis of symmetric fracture mirrors in glass bottles. *Int. J. Fract.* **18**, 29–38.

Bansal, G. K. 1977. On fracture mirror formation in glass and polycrystalline ceramics. *Phil. Mag.* **35**, 935–944.

Bansal, G. K. & Duckworth, W. H. 1977. Fracture stress in related flaw and fracture mirror sizes. *J. Am. Ceram. Soc.* **60**, 304–310.

Bankwitz, V. P. 1966. Die bildung der kluftflache und eine systematik ihrer strukturen. *Uber Klufte Geol.* **15**, 896–941.

Brace, W. F. & Walsh, J. B. 1962. Some direct measurements of the surface energy of quartz and orthoclase. *Am. Miner.* **47**, 1111–1122.

Bryant, P. J., Taylor, L. H. & Gutshall, P. L. 1963. Cleavage studies of lamellar solids in various gaseous environments. *Trans. 10th Ann. natl Vacuum Symposium*, American Vacuum Society, 21–26.

Charles, R. J. 1958. Dynamic fatigue of glass. *J. appl. Phys.* **29**, 1657–1662.

Congleton, J. & Petch, N. J. 1967. Crack-branching. *Phil. Mag.* **16**, 749–760.

Friedman, M. & Logan, J. M. 1970. Influence of residual elastic strain on the orientation of experimental fractures in three quartzose sandstones. *J. geophys. Res.* **75**, 387–405.

Garfunkel, Z. & Bartov, Y. 1977. The tectonics of the Suez rift. *Bull. Geol. Surv. Isr.* **71**, 44.

Hodgson, R. A. 1961. Regional study of jointing in Comb Ridge Navajo Mountain area, Arizona and Utah. *Bull. Am. Ass. Petrol. Geol.* **45**, 1–38.

Holloway, D. G. 1973. *The Physical Properties of Glass*. Wykeham Publications, London.

Kobayashi, A. S., Wade, B. G., Bradley, W. B. & Chiu, S. T. 1974. Crack branching in Homalite-100 sheets. *Engng Fract. Mech.* **6**, 81–92.

Kohn, B. P. & Eyal, M. 1981. History of uplift of the crystalline basement of Sinai and its relation to opening of the Red Sea as revealed by fission track dating of apatites. *Earth Planet. Sci. Lett.* **52**, 129–141.

Kulander, B. R., Barton, C. C. & Dean, S. L. 1979. The application of fractography to core and outcrop fracture investigations. *METC/SP-79/3 distribution category UC-92a.*

McGill, G. E. & Stromquist, A. W. 1979. The grabens of Canyon Lands National Park, Utah: geometry, mechanics and kinematics. *J. geophys. Res.* **84**, 4547–4563.

Mecholsky, J. J. & Frieman, S. W. 1979. Determination of fracture mechanics parameters through fractographic analysis of ceramics. In: *Fracture Mechanics Applied to Brittle Materials* (edited by Freiman, S. W.). *ASTM Spec. Tech. Pub.* **678**, 136–150.

Mould, R. E. & Southwick, R. E. 1959. Strength and static fatigue of abraded glass under controlled ambient conditions: II. Effect of various abrasions and the universal fatigue curve. *J. Am. Ceram. Soc.* **42**, 582–592.

Norton, H. G. & Atkinson, B. K. 1981. Stress-dependent morphological features on fracture surfaces of quartz and glass. *Tectonophysics* **77**, 283–295.

Peck, L., Nolon-Hoeksema, R. C., Barton, C. C. & Gordon, R. B. 1985. Measurement of the resistance of imperfectly elastic rock to the propagation of tensile cracks. *J. geophys. Res.* **90**, 7827–7836.

Randall, P. N. 1966. *Plane Strain Crack Toughness Testing of High Strength Metallic Materials* (edited by Brown, W. F. Jr & Sawley, J. E.). *ASTM Spec. Tech. Pub.* **410**, 88–129.

Secor, Jr. D. T. 1969. Mechanisms of natural extension fracturing at depths in the earth's crust. *Geol. Surv. Pap. Can.* **68–52**, 3–48.

Segall, P. & Pollard, D. D. 1983. Joint formation in granitic rock of the Sierra Nevada. *Bull. geol. Soc. Am.* **94**, 563–575.

Voight, B. & St. Pierre, B. H. P. 1974. Stress history and rock stress. *Proc. 3rd Rock Mech. Congr-ISRM* **2**, 580–582.

Wiederhorn, S. M. 1967. Influence of water vapor on crack propagation in soda-lime glass. *J. Am. Ceram. Soc.* **50**, 407–414.

Wiederhorn, S. M., Evans, A. G., Fuller, E. R. & Johnson, H. 1974. Application of fracture mechanism to space-shuttle windows. *J. Am. Ceram. Soc.* **57**, 319–323.

Wilkins, B. J. S. 1980. Slow crack growth and delayed failure of granites. *Int. J. Rock Mech. & Mining Sci.* **17**, 365–369.

Woodworth, J. B. 1896. On the fracture system of joints, with remarks on certain great fractures. *Boston Soc. natl Hist. Proc.* **27**, 163–183.